ELSEVIER

Journal of Nuclear Materials 252 (1998) 187–194

journal of nuclear materials

A theoretical model for determination of fracture toughness of reactor pressure vessel steels in the transition region from automated ball indentation test

Thak Sang Byun *, Jin Weon Kim, Jun Hwa Hong

Reactor Material Department, Korea Atomic Energy Research Institute, Yusong P.O.Box 105, Taejon 305-600, South Korea

Received 11 August 1997; accepted 27 October 1997

Abstract

A theoretical model is proposed to estimate the fracture toughness of ferritic steels in the transition region from ball indentation test data. The key concept of the model is that the indentation energy to a critical load is related to the fracture energy of the material. By applying the new model, the fracture parameters of reactor pressure vessel steel base and weld metals were estimated from the indentation load–depth curves. The estimated fracture stresses agreed well with those of the Wilshaw et al. model. The temperature dependence of the estimated K_{JC} was almost the same as that of the ASTM K_{JC} master curve. Also, the reference temperature obtained from the estimated K_{JC} versus temperature curve correlated well with the index temperature of 41 J Charpy impact energy, $T_{41\,J}$. Additionally, the ball indentation deformation was simulated by ABAQUS code to evaluate the stress state and the result was compared with that at the crack tip. © 1998 Elsevier Science B.V.

1. Introduction

In the assessment of structural material integrity, the automated ball indentation (ABI) test is an attractive test technique to obtain material property data because it is in nature semi-nondestructive and requires a relatively small material volume [1]. Furthermore, the ABI technique makes it possible to perform portable/in situ tests on in-service components such as reactor pressure vessels (RPV) and power plant pipelines. Many theories and models have been developed to measure the mechanical properties of materials with ball indentation techniques [2–7], and some fundamental mechanical properties, such as yield and ultimate strengths and stress–strain curves can be measured by the current ABI test technology [8,9].

When assessing the integrity of structural materials, fracture toughness is considered as the most important parameter. Most of the structural materials are ductile metals. However, the ball indentation on the ductile metals rarely induces cracking. For this reason, the estimation of fracture toughness using the indentation test has been rarely attempted for the ductile metals [8]. The objective of this work is to develop a methodology for estimating the fracture toughness of ferritic steels from the ABI test data.

In Section 2, a theoretical model is proposed on the concept that the indentation deformation energy per unit contact area to a critical load is related to the fracture energy per unit area. The fracture energy per unit area is divided into two terms: a temperature-independent term (= lower shelf energy) and a temperature-dependent term. In the proposed model, it is assumed that the indentation energy per unit contact area is identical to the temperature-dependent term. To impose a criterion for imaginary fracture on the indentation deformation, it is assumed that fracture occurs when the maximum contact pressure reaches the fracture stress of the material. Also, the concepts of temperature-independent cleavage fracture stress [10,11] and Meyer law [2–4,7] are incorporated.

This paper also includes the application results for RPV steels including five base metals (SA508 Gr.3 steels) and four weld metals. Additionally, the indentation deforma-

* Corresponding author. Tel.: +82-42 868 2421; fax: +82-42 868 8346; e-mail: tsbyun@nanum.kaeri.re.kr.

PII S0022-3115(97)00338-3

tion was simulated by a finite element method (FEM) code and the stress state was analyzed.

2. Theoretical model

The fracture toughness can be defined as resistance to the propagation of crack. Therefore the cracked specimen has been used to measure it. Under an external load, highly concentrated stress and strain fields are generated ahead of crack tip and the degree of the stress concentration depends on the constraint effect of the crack [11–14]. Indentation into a sample with a small indenter may also produce a deformation field concentrated highly around the contact of the indenter and sample. Since only a small amount of volume is deformed by the indentation, the deformation may be highly constrained by the surrounding material. Preliminary computer simulations showed that the degree of constraint in the deformed volume was similar to that ahead of crack tip. In this work, the fracture energy is interpreted as the deformation capability of the material under a highly constrained stress field. Based on this concept, we attempted to correlate the indentation deformation energy with the fracture energy and consequently the fracture toughness.

There are also distinct differences between the indentation deformation and the deformation ahead of crack tip. First, the principal stress components within the edge of impression are compressive, while those around the crack tip are tensile. However, generally it is accepted that the compressive and tensile deformations are equivalent if the deformation is not cyclic; in the case of cyclic loading, the Baushinger effect reduces the strength on reversed deformation. Secondly, the material failure consists of deformation and cracking. On ductile metals, however, the indentation with a usual ball indenter would not induce cracking even at lower shelf temperatures. In the following theory, an imaginary fracture is introduced to the indentation deformation in order to determine a critical point of deformation corresponding to the cracking.

2.1. Indentation energy to fracture (IEF)

With the above background, we postulate that the indentation energy per unit contact area to a critical load is related to the fracture energy of the material. Hereafter, that energy is referred to as the indentation energy to fracture (IEF) and defined as

$$W_{\mathrm{IEF}} = \frac{4}{\pi d_{\mathrm{f}}^2}\int_0^{h_{\mathrm{f}}} P\,\mathrm{d}h, \tag{1}$$

where P is the applied load, h is the indentation depth, h_{f} is the critical indentation depth and d_{f} is the critical chordal diameter of impression. RPV steels usually reveal an almost linear indentation load–depth (P–h) curve; $P = Sh$, where S is the slope of the curve. Thus, integrating Eq. (1) to the critical point,

$$W_{\mathrm{IEF}} = \frac{2}{\pi S}\left(\frac{P_{\mathrm{f}}}{d_{\mathrm{f}}}\right)^2, \tag{2}$$

where P_{f} is the critical load.

To obtain the critical load and critical chordal diameter, a criterion for imaginary fracture is imposed to the indentation deformation; the test material is assumed to fracture when the maximum contact pressure of indentation impression, $p_{\max}$, reaches fracture stress, σ_{f}:

$$p_{\max} = \sigma_{\mathrm{f}}. \tag{3}$$

Defining the ratio of the maximum contact pressure to the mean contact pressure as μ, the criterion for fracture becomes

$$p_{\max} = \mu p_{\mathrm{m}}^{\mathrm{f}}, \tag{4}$$

where $p_{\mathrm{m}}^{\mathrm{f}}$ is the critical mean contact pressure, which is the mean contact pressure at critical load.

Using the definition of mean contact pressure:

$$p_{\mathrm{m}}^{\mathrm{f}} = \frac{4P_{\mathrm{f}}}{\pi d_{\mathrm{f}}^2} \tag{5}$$

and Meyer law [2–4,7]:

$$\frac{P_{\mathrm{f}}}{d_{\mathrm{f}}^2} = A\left(\frac{d_{\mathrm{f}}}{D}\right)^{m-2}, \tag{6}$$

where A is the material yield parameter, m is the Meyer index and D is the ball diameter. The critical chordal diameter and critical load are, respectively, given by

$$d_{\mathrm{f}} = D\left(\frac{\pi p_{\mathrm{m}}^{\mathrm{f}}}{4A}\right)^{1/(m-2)}, \tag{7}$$

$$P_{\mathrm{f}} = AD^2\left(\frac{\pi p_{\mathrm{m}}^{\mathrm{f}}}{4A}\right)^{m/(m-2)}. \tag{8}$$

Inserting Eqs. (7) and (8) into Eq. (2), the IEF is expressed by

$$W_{\mathrm{IEF}} = \frac{2A^2D^2}{\pi S}\left(\pi\frac{p_{\mathrm{m}}^{\mathrm{f}}}{4A}\right)^{(2m-2)/(m-2)} \tag{9a}$$

or

$$W_{\mathrm{IEF}} = \frac{2A^2D^2}{\pi S}\left(\frac{\pi\sigma_{\mathrm{f}}}{4\mu A}\right)^{(2m-2)/(m-2)}. \tag{9b}$$

The toughness parameters, such as Charpy impact energy and static fracture toughness, K_{JC}, have non-zero lower shelves, even at very low temperatures. Thus the fracture energy per unit area, W_{f}, can be given by

$$W_{\mathrm{f}} = W_0 + W_{\mathrm{T}}, \tag{10}$$

where W_0 is the lower shelf energy per unit area, determined by the fracture surface formation energy and pure elastic energy and W_T is the temperature-dependent energy per unit area. The latter term might be related to the elastic–plastic deformation and becomes a larger portion of the total fracture energy at the transition temperatures. Since W_{IEF} includes only elastic–plastic deformation energy, it is regarded as the temperature-dependent energy: $W_T = W_{IEF}$.

2.2. Fracture stress

Fracture stress can be obtained through the notched bar specimen tests [15,16] or calculated from fracture toughness and yield stress data using fracture mechanics models [17–19]. In the present work, however, it is attempted to estimate the fracture stress from ABI test data and existing K_{JC} data by coupling the IEF theory with fracture mechanics models [20,21].

For a crack of length $2a$ in infinite plate, fracture toughness is given by [20]

$$K_{JC} = \sigma_F \sqrt{\pi a}\,, \tag{11}$$

where σ_F is the remote tensile stress at fracture, which is normal to the crack surface. According to the generalized Griffith theory [20], σ_F is

$$\sigma_F = \sqrt{\frac{2EW_f}{\pi a}}\,. \tag{12}$$

Eliminating a from Eqs. (11) and (12), the relationship between fracture energy and fracture toughness becomes

$$W_f = \frac{K_{JC}^2}{2E}\,. \tag{13}$$

Then, this relationship can determine W_f when K_{JC} is known.

For the ferritic steels, the fracture toughness (median value) versus temperature curve in the transition temperature region is expressed by the master curve [22]

$$K_{JC}(\text{med}) = 30 + 70e^{0.019(T-T_0)}, \quad \text{MPa}\sqrt{\text{m}}\,, \tag{14}$$

where T_0 is the reference temperature (the temperature when $K_{JC} = 100$ MPa $\sqrt{\text{m}}$). In this curve, the lower shelf of fracture toughness is 30 MPa $\sqrt{\text{m}}$. Accordingly, the lower shelf energy, W_0, is calculated at 2143 J/m^2 by Eq. (13), where $E = 210$ GPa. With Eqs. (9a), (9b) and (13) the fracture stress (or critical mean contact pressure) is calculated from the K_{JC} data, ABI data and W_0, as follows:

$$\sigma_f = \mu p_m^f = \frac{4\mu A}{\pi}\left[\frac{\pi S(W_f - W_0)}{2A^2D^2}\right]^{(m-2)/(2m-2)}. \tag{15}$$

3. Application and analysis

3.1. Indentation test

The test materials comprise of five SA508 Gr.3 RPV base metals and four RPV weld metals. Table 1 contains the chemical compositions of the steels. The base metals are in a quenched, tempered and post-weld heat-treated state and the weld metal is in a post-weld heat-treated state. The Charpy-sized rectangular bars ($10 \times 10 \times 55$ mm) cut from the 1/4 thickness locations of RPVs were used in the ABI tests.

Continuous indentation tests were performed in an ABI test system of Advanced Technology Corporation (model: PortaFlow-P1). The indenter used was a tungsten carbide (WC) ball of 0.508 mm diameter. A specially designed bath was installed on the ABI test system for low temperature tests, in which the test temperature was controlled by liquid nitrogen with an accuracy of ± 2°C. The indentation tests were performed at temperatures of -150 to 0°C with an indentation speed of 0.0076 mm/s (0.0003 inch/s), which gives an average strain rate of about 10^{-2} s^{-1} for the deformed region.

Table 1
Chemical compositions of SA508 Gr.3 RPV steels and weld metals

Material	Chemical composition (wt%)										Remarks
	C	Mn	Si	Al	Ni	Cr	Mo	P	S	Cu	
HB1	0.17	1.39	0.08	0.004	0.77	0.04	0.49	0.007	0.003	0.05	base metal
HB2	0.20	1.42	0.07	0.005	0.79	0.15	0.57	0.007	0.003	0.06	base metal
HB3	0.17	1.41	0.06	0.006	0.84	0.15	0.51	0.006	0.002	0.03	base metal
HB4	0.19	1.35	0.09	0.009	0.82	0.16	0.52	0.008	0.004	0.04	base metal
HB5	0.21	1.36	0.24	0.022	0.92	0.21	0.49	0.007	0.002	0.03	base metal
HW1	0.07	1.73	0.22	0.009	0.07	0.05	0.52	0.015	0.004	0.02	weld metal
HW2	0.07	1.69	0.26	0.01	0.11	0.06	0.53	0.016	0.004	0.02	weld metal
HW3	0.08	1.72	0.29	0.01	0.18	0.06	0.50	0.009	0.002	0.03	weld metal
HW4	0.08	1.74	0.26	0.01	0.13	0.05	0.51	0.011	0.002	0.03	weld metal

3.2. Calculation of fracture parameters

It has been known that the cleavage fracture stress of ferritic steels is nearly independent of temperature in the low temperature region [10,11]. Eqs. (3) and (4) state that the critical mean contact pressure, p_m^f, also can be regarded as a temperature-independent parameter. By using Eq. (15), p_m^f was calculated from the ABI test data and low-temperature K_{JC} data. To assure that the fracture stress is temperature-independent, the K_{JC} data obtained at temperatures lower than -20°C were taken into account; in this low temperature region the test materials revealed cleavage fracture without stable crack growth. 2–4 critical mean contact pressure data were obtained for each test material. The average of those was used as a material constant of each material in the calculation of IEF.

A and S were strongly dependent on test temperature and were therefore calculated from the indentation load–depth data for each test temperature. The values of m (Meyer index), about 90 data, were obtained by regression of the load–chordal diameter (P–d) data. The average value of m was about 2.14 and the standard deviation was about 0.043. Since m is insensitive to temperature and test material, the average value, 2.14, was applied to all calculations.

It is necessary to evaluate μ to obtain the fracture stress from the critical mean contact pressure, as indicated in Eqs. (3) and (4). ABAQUS code simulation showed that the μ value in the plastic deformation ranged from 1 to 1.2. The average value of 1.1 was used for the calculation of fracture stress.

3.3. Computer simulation of indentation deformation

ABAQUS code was used to simulate the indentation deformation of HB2 steel by the ball indenter of 0.508 mm diameter under room temperature condition. The deformed region due to ball indentation has an axi-symmetrical geometry; thus a two-dimensional finite element array was modeled on the plane of circumferential direction. The linear quadrilateral elements of two sizes were used; 5 μm mesh was used for the region near the ball-specimen contact and 15 μm mesh for the region away from the contact. Also, a trapezoidal element was incorporated for connecting the two regions. Hereafter, the radial, axial (or loading) and circumferential directions are denoted by x-, y-, z-directions, respectively. Since the deformation is axi-symmetrical, the displacement in the x-direction was set to be zero at the centerline nodes. Also, the displacement in the y-direction was set to be zero at the bottom nodes.

The test material was assumed to be elastically and plastically isotropic. Poisson's ratio (ν) was 0.28 and Young's modulus (E) was 200 GPa. Power-law hardening was assumed for the material analyzed; therefore, the true stress–true strain curve was expressed by the Hollomon equation: $\sigma = 1025\varepsilon^{0.12}$, which was obtained by ABI testing. The von Mises expression was used in the calculation of equivalent stress. The ball indenter was assumed to be rigid.

With the above assumptions and boundary conditions, iterative calculations were carried out to determine the friction coefficient at the contact of the WC ball indenter and RPV steel. The difference between the calculated and measured load–depth curves was minimized when the friction coefficient was about 0.1. This value was applied to the simulation for the representative case. A super computer (CRAY-90) was used to run the ABAQUS code.

4. Results and discussion

4.1. Critical mean contact pressure and fracture stress

The temperature dependence of critical mean contact pressure, p_m^f, is illustrated in Fig. 1. For all test materials, no significant temperature dependence is observed in the temperature region of -110 to -20°C. This result confirms the assumption of temperature-independent fracture stress in the low temperature region. Table 2 contains the averages of critical mean contact pressure data. Also, the fracture stress, σ_f, was calculated by $1.1\,p_m^f$, as listed in Table 2. The fracture stresses of base metals are in the range of 2500 to 2800 MPa and those of weld metals are in the range of 2800 to 3100 MPa. These values are close to those of the steels with similar microstructures; 2130 to 2250 MPa for A533B steels [18,23], 2270 to 2450 MPa for C–Mn base and weld metals and Ti–B weld metals [15] and 2100 to 2900 MPa for quenched and tempered steels manufactured by various heat treatment conditions [16]. For the purpose of comparison, the fracture stress (in MPa)

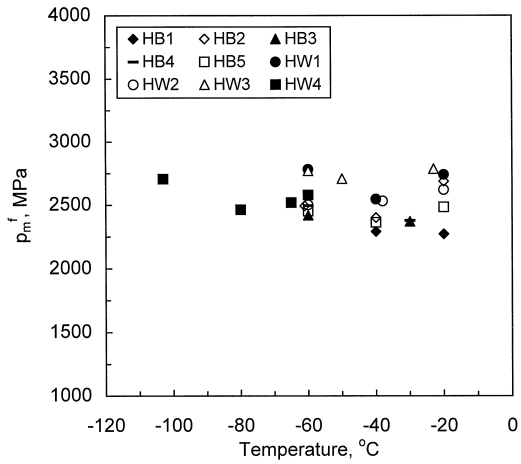

Fig. 1. Critical mean contact pressure versus temperature.

Table 2
Critical mean contact pressure and fracture stress

Material	p_m^f from Eq. (15)	$\sigma_f = 1.1\, p_m^f$	σ_f^* from Eq. (16)	σ_f / σ_f^*
HB1	2282	2510	2590	0.97
HB2	2527	2780	2778	1.00
HB3	2396	2636	2699	0.98
HB4	2437	2681	3044	0.88
HB5	2433	2676	2879	0.93
HW1	2690	2959	3031	0.98
HW2	2552	2807	2747	1.02
HW3	2754	3029	2898	1.05
HW4	2567	2824	2890	0.98

was calculated by the Wilshaw et al. fracture mechanics model [17–19]:

$$\sigma_f^* = \sigma_y \left[1 + \ln\left(1 + 2360 \left(\frac{K_{IC}}{\sigma_y} \right)^2 \right) \right], \qquad (16)$$

where σ_y is the yield stress. This relationship was derived from the stress distribution ahead of the crack tip. For each material, σ_f^* was evaluated for the reference temperature and compared with the σ_f value in Table 2. The ratios of σ_f to σ_f^* are close to unity; the fracture stress estimated by IEF theory agrees well with that of the Wilshaw et al. model.

4.2. Fracture toughness transition curve

The fracture toughness, K_{JC}, was calculated with Eqs. (9a), (10) and (13) and the transition temperature curves, called master curves, were obtained by regression of the estimated K_{JC} data for -150 to 0°C. According to the master curve method [22], the temperature transition of fracture toughness can be described by one parameter: the reference temperature, T_0. This is because the other coefficients of the curve are nearly the same for whole ferritic steels, as indicated in Eq. (14). Then, all master curves of different ferritic steels will overlap on one curve if the independent variable is given by the temperature relative to T_0; $T - T_0$.

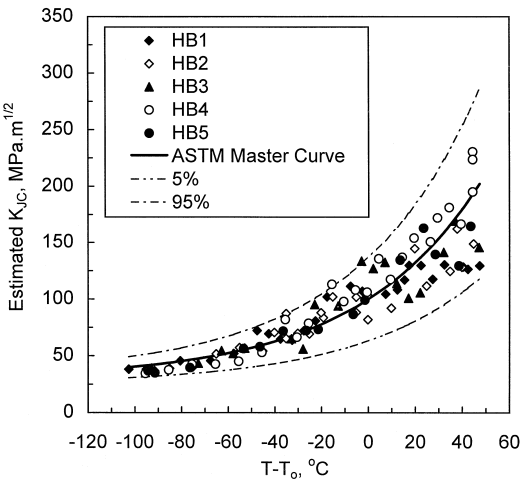

Fig. 2. Estimated K_{JC} of SA508 Gr.3 steels (base metals).

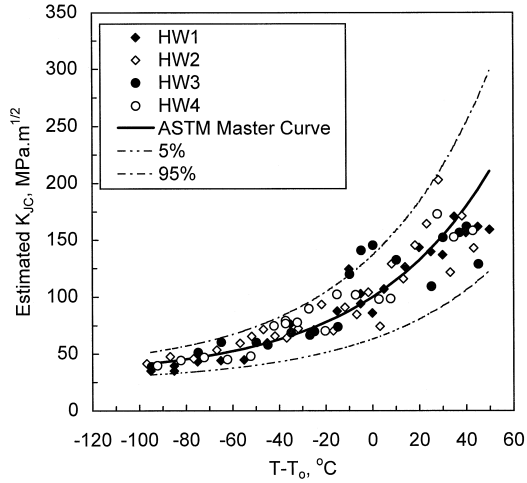

Fig. 3. Estimated K_{JC} of RPV weld metals.

The estimated K_{JC} values are illustrated in Figs. 2 and 3 with the ASTM master curve (K_{JC}(median) versus $T - T_0$) and two bounding curves (dotted) of 5 and 95% fracture probabilities. Most estimated K_{JC} data are within the two dotted curves. Also, Table 3 shows that the coefficient q of the temperature transition curves are in the range of 0.0166 to 0.0218. The average is 0.0194, which is very close to that of the ASTM K_{JC} master curve: 0.019. This parameter determines the shape of fracture toughness transition curves and the reference temperature, T_0, determines the position of the curve in the temperature axis. Therefore, it can be concluded that the temperature transi-

Table 3
Parameters of estimated fracture toughness master curves

Fracture toughness master curve:
$K_{JC}(T) = 30 + 70e^{q(T - T_0)}$ MPa $\sqrt{m}$

material	q	T_0
HB1	0.0206	−32.4
HB2	0.0196	−40.0
HB3	0.0218	−37.1
HB4	0.0215	−64.5
HB5	0.0181	−88.6
HW1	0.0193	−74.9
HW2	0.0166	−53.2
HW3	0.0189	−45.2
HW4	0.0186	−57.8
	Average = 0.0194	

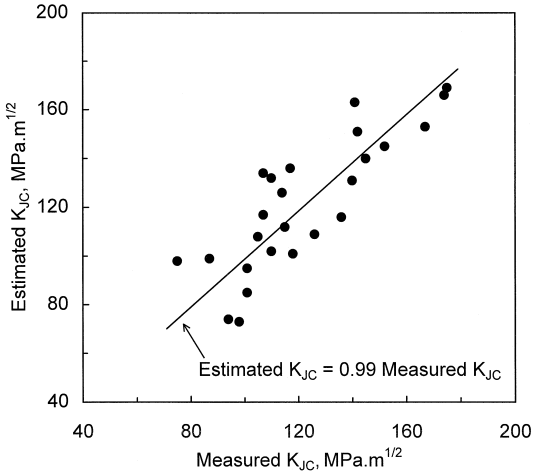

Fig. 4. Comparison of estimated K_{JC} with measured K_{JC}.

tion behavior of the estimated K_{JC} is almost the same as that of the ASTM K_{JC} master curve.

In Fig. 4 the estimated K_{JC} data are compared with the K_{JC} data obtained from 1T-CT (compact tension) or 1/2T-CT specimens. In Fig. 4 to exclude the data of upper transition temperatures, only K_{JC} values less than 200 MPa $\sqrt{m}$ are included. Although Fig. 4 shows a large data scattering, there is a good linear proportionality between the estimated K_{JC} and the measured K_{JC}.

On the other hand, Fig. 5 shows the comparison of T_0 and $T_{41\ J}$ (the index temperature when Charpy impact energy is 41 J). The two transition temperatures are linearly proportional to each other. It is worth noting that the fitted curve reveals a cut-off value of -31.1°C. This may be originated from the differences in the strain rate (or loading rate) and stress state between the two tests. In general, the fracture stress is reduced by increasing the strain rate or by decreasing the stress triaxiality [15]. Consequently, reduction in the fracture stress may shift the transition temperature toward a higher temperature.

4.3. Stress state

In notched or cracked specimens, the stress state ahead of crack tip affects fracture behaviors [13,24–28]. The stress state has been described frequently by the stress triaxiality:

$$t = \frac{\sigma_m}{\sigma_{eq}}, \tag{17}$$

where σ_m is the mean stress and σ_{eq} is the equivalent stress (= effective flow stress). These stresses are defined, respectively, by

$$\sigma_m = \frac{(\sigma_{xx} + \sigma_{yy} + \sigma_{zz})}{3}, \tag{18}$$

$$\sigma_{eq} = \left(\frac{1}{\sqrt{2}}\right)\left[(\sigma_{xx} - \sigma_{yy})^2 + (\sigma_{yy} - \sigma_{zz})^2 + (\sigma_{zz} - \sigma_{xx})^2\right]^{1/2}, \tag{19}$$

where σ_{yy} is defined as the stress in the loading direction, which is the maximum stress component and σ_{xx} and σ_{zz} as the transverse components.

By using the same definitions as Eqs. (17)–(19) the stress triaxiality in the indentation deformation was calculated from the stress components at the center of the impression. The variation in the stress triaxiality is presented in Fig. 6 as a function of normalized indentation depth, h/R, where R is the ball radius. The stress triaxiality is about 2 at the initiation of indentation at which the

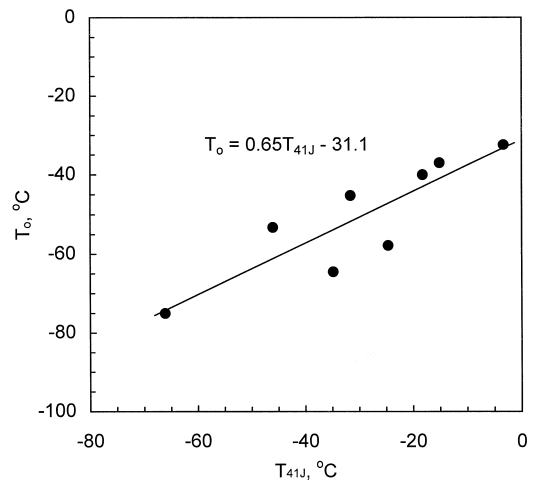

Fig. 5. Correlation between the reference temperature, T_0, and the index temperature of the Charpy impact energy, $T_{41\ J}$.

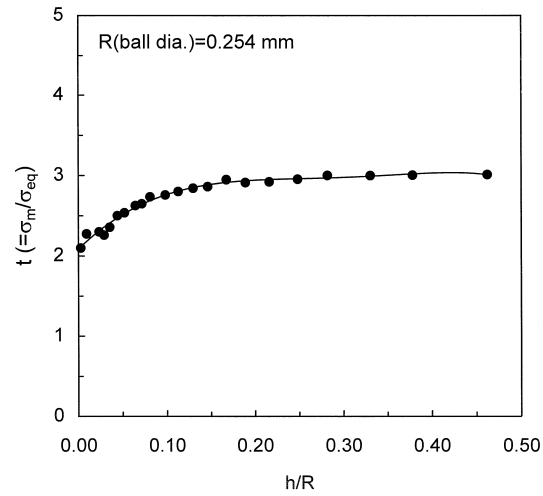

Fig. 6. Variation of stress triaxiality at the center of impression with normalized indentation depth.

Table 4
Comparison of stress state

Case	Stress triaxiality (t)
Continuous ball indentation (at the center of impression, 0.508 mm diameter ball)	2–3
Elastic fields at crack tip ($\nu = 0.28$, from Eq. (20))	1.94
HRR fields at crack tip ($n = 0.1$ from Eq. (21))	3.3
Pre-cracked CT (simulation by FEM) [13] (maximum value ahead of crack tip, various n and load levels)	1.7–3.2
Pre-cracked CT (simulation by FEM) [27] (maximum value ahead of crack tip, RPV steels, various load levels)	1.8–2.8
Pre-cracked COD (simulation by FEM) [28] (maximum value ahead of crack tip, low alloy steels,at critical fracture points, at low temperatures)	1.8–3
Notched round bars at notch root [26]	0.6–2.2
Smooth tensile specimen (for uniaxial stress)	0.33

test material may be deformed elastically only. The stress triaxiality increases up to about 3 as the indentation depth increases and nearly saturates when h/R reaches about 0.2. This result implies that the stress state of indentation deformation is much severer than that of the smooth tensile specimen under uniaxial load, whose stress triaxiality is only about 0.33.

Furthermore, the stress triaxiality values for various cases are listed in Table 4. Under the plane strain condition of $\sigma_{zz} = \nu(\sigma_{xx} + \sigma_{yy})$ the lower bound of the stress triaxiality ahead of crack tip (for $\theta = 0$) can be derived from the elastic fields [29] as

$$t_{\text{elastic}} = \frac{2(1+\nu)}{3(1-2\nu)}. \tag{20}$$

For elastic–plastic deformation, an expression for the stress triaxiality at crack tip ($\theta = 0$) can be obtained from the HRR (Hutchinson, Rosengren and Rice) stress fields [30]:

$$t_{\text{HRR}} = \frac{(1+\pi)}{\sqrt{3}} e^{3.1n}, \tag{21}$$

where n is the strain-hardening exponent in the power–law curve. Since the relaxation at the crack tip is ignored in the HRR fields, t_{HRR} can be regarded as an upper bound of the stress triaxiality at the crack tip. Eq. (21) implies that the maximum stress triaxiality is determined by the strain-hardening capability of the material [13]. Finite element simulations [13,27,28] confirm these analytical bounds, as shown in Table 4. Comparing the indentation deformation with the deformation ahead of crack tip, we can recognize that fairly similar stress triaxialities are found for the two deformations. It is also worth noting that the stress triaxiality depends strongly on the kind of specimen and is a function of position and degree of deformation (or blunting of crack).

According to the fracture mechanics model [16], the fracture toughness is proportional to the square root of the fracture stress and fracture strain. The fracture stress is determined by the maximum magnification of the principal stress ahead of crack tip, which is proportional to the stress triaxiality [14–19,28,31]. Since the fracture stress of ferritic steels in the low temperature region is nearly temperature-independent, the temperature transition of fracture toughness may be mainly dependent on the transition behavior of the fracture strain. The fracture strain is defined by the local strain when the maximum principal stress reaches the fracture stress of the material, and therefore the fracture strain is also determined by the degree of stress triaxiality [24–26]. Accordingly, a similar degree of stress triaxiality is required to obtain similar fracture toughness values from different tests. As shown in Section 4.2 the estimated K_{JC} values are close to those measured by the fracture tests using the pre-cracked CT specimens. We conclude that this result is attributed to the common feature in the stress state of the two tests.

5. Conclusions

A methodology for estimating the fracture toughness in the transition region from ball indentation test data is suggested and is applied to the evaluation of RPV steels. The results are summarized as follows.

(1) The fracture stresses estimated were in the range of 2500 to 2800 MPa for base metals and in the range of 2800 to 3100 MPa for weld metals. These values agreed well with the values calculated by fracture mechanics model.

(2) The temperature dependence of estimated K_{JC} was well described by the function of the form: $e^{q(T-T_0)}$, where all q values were in the range of 0.0166 to 0.0218 and their average was 0.0194. This means that the temperature dependence of estimated K_{JC} is almost the same as that of the ASTM K_{JC} master curve.

(3) The reference temperature, T_0, of the steels was determined from the estimated K_{JC} versus temperature curve. The reference temperature correlated well with the index temperature of the Charpy impact energy, $T_{41\text{ J}}$.

(4) Additionally, computer simulation on the indentation stress and strain fields was performed to explain the above application results in terms of the stress state. The indentation deformation reveals a very similar degree of stress triaxiality to the deformation ahead of crack tip.

Acknowledgements

The authors would like to thank Dr B.S. Lee, Mr J.H. Yoon and Mr J.H. Kim for supplying the fracture test and impact test data. This work is a part of the Advanced Nuclear Materials Development Program/Nuclear Structural Steels, which has been financially supported by the Korean Ministry of Science and Technology.

References

[1] F.M. Haggag, R.K. Nanstad, D.N. Braski, in: D.L. Mariott, T.R. Mager, W.H. Bamford (Eds.), Innovative Approaches to Irradiation Damage and Fracture Analysis, vol. 170, ASME PVP, 1989, pp. 101–107.
[2] E. Meyer, Z. Ver. Dtsch Ing. 52 (1908) 645.
[3] E. Meyer, Z. Ver. Dtsch Ing. 52 (1908) 740.
[4] E. Meyer, Z. Ver. Dtsch Ing. 52 (1908) 835.
[5] R.A. George, S. Dinda, A.S. Kasper, Met. Prog. (1976) 30.
[6] H.A. Francis, J. Eng. Mater. Technol. 98 (3) (1976) 272.
[7] D. Tabor, J. Inst. Met. 79 (1951) 1.
[8] F.M. Haggag, in: W.R. Corwin, F.M. Haggag, W.L. Server (Eds.), Small Specimen Test Techniques Applied to Nuclear Reactor Vessel Thermal Annealing and Plant Life Extension, ASTM STP 1204, 1993, p. 27.
[9] T.S. Byun, J.H. Kim, S.H. Chi, J.H. Hong, Proc. 6th Symp. on Mater. Degradation and Life Prediction, Seoul, Korea, 1996, p. 167.
[10] R. Sandstrom, Y. Bergstrom, Met. Sci. 18 (1984) 177.
[11] J. Heerens, D.T. Read, A. Cornec, K.H. Schwalbe, in: J.G. Blauel, K.H. Schwalbe (Eds.), Defect Assessment in Components: Fundamentals and Applications, Mech. Engi. Pub., London, 1991, p. 659.
[12] T.L. Anderson, R.H. Dodds Jr., J. Testing Eval. 19 (2) (1991) 123.
[13] G. Wanlin, Eng. Fract. Mech. 51 (1) (1995) 51.
[14] D. Aurich, E. Sommer, Steel Res. 59 (8) (1988) 358.
[15] J.H. Chen, H. Ma, G.Z. Wang, Metal. Trans. 21A (1990) 313.
[16] Z. Xiulim, Eng. Fract. Mech. 33 (5) (1989) 685.
[17] T.R. Wilshaw, C.A. Rau, A.S. Tetelman, Eng. Fract. Mech. 1 (1968) 191.
[18] J. Markin, A.S. Tetelman, Eng. Fract. Mech. 3 (1971) 151.
[19] R.O. Ritchie, J.F. Knott, J.R. Rice, J. Mech. Phys. Solids 21 (1973) 395.
[20] T.L. Anderson, Fracture Mechanics, CRC, Boca Raton, FL, 1995, p. 41.
[21] H.K. Oh, Eng. Fract. Mech. 55 (1996) 865–868.
[22] ASTM Standard Draft 13, Test method for the determination of reference temperature, T_0, for ferritic steels in the transition range, Rev. 7-1-1997.
[23] J.F. Knott, Micro-mechanisms of Plasticity and Fracture, University of Waterloo Press, 1983, pp. 261–302.
[24] A.C. Mackenzie, J.W. Hancock, D.K. Brown, Eng. Fract. Mech. 9 (1977) 167.
[25] M. Zheng, X. Zheng, Theor. Appl. Fract. Mech. 18 (1993) 157.
[26] M.S. Mirza, D.C. Barton, P. Church, J. Mater. Sci. 31 (1996) 453.
[27] H. Kordisch, E. Sommer, W. Schmitt, Nucl. Eng. Design 112 (1889) 27.
[28] G.Z. Wang, J.H. Chen, Metal. Trans. 27A (1996) 1909.
[29] K. Kellan, in: Eichberg (Ed.), Introduction to Fracture Mechanics, McGraw-Hill, 1984, p. 7.
[30] J.R. Rice, G.F. Rosengren, J. Mech. Phys. Solids 16 (1968) 1.
[31] R.O. Ritchie, W.L. Server, R.A. Wullaert, Metall. Trans. 10A (1979) 1557.